Study of the influence of recycling aluminum on the cyclic material behavior for chill cast AlSi7Mg0.3

Christoph Bleicher, Ahmad Qaralleh
Fraunhofer Institute for Structural Durability and System Reliability LBF, Germany
christoph.bleicher@lbf.fraunhofer.de, http://orcid.org/0000-0002-0874-9548
ahmad.qaralleh@lbf-extern.fraunhofer.de, http://orcid.org/0009-0009-9043-1720

Sascha Fliegener, Silke Sommer
Fraunhofer Institute for Mechanics of Materials IWM, Germany
sascha.fliegener@iwm.fraunhofer.de, http://orcid.org/0009-0000-6469-744X
silke.sommer@iwm.fraunhofer.de, http://orcid.org/0009-0001-9375-560X

Robert Kleinhans, Manuel Pintore
Fraunhofer Institute for Casting, Composite and Processing Technology IGCV, Germany
robert.kleinhans@igcv.fraunhofer.de, http://orcid.org/0009-0004-0391-2539
manuel.pintore@igcv.fraunhofer.de, http://orcid.org/0000-0002-9082-3742

ABSTRACT. Automotive industry and mechanical engineering strive to drastically reduce the carbon footprint of their products. This becomes increasingly important as aluminum usage grows for lightweight, efficient components. Nevertheless, cast aluminum products suffer from a lack of alloys bearing higher fractions of recycling content, though their availability is crucial. Using recycling aluminum in gravity die casting offers high potential for CO_2 reduction, but the effect of increasing accompanying elements like Cu, Zn or Fe on cyclic material behavior has not been investigated yet.
Within the Fraunhofer internal research project "FutureCarProduction," the effects of secondary aluminum alloys on casting processes as well as fatigue and crash behavior of car body components are investigated. The aim is to find the optimal combination between manufacturing efficiency and durability regarding the alloy's potential to reduce carbon footprint and emissions during the product life cycle.

Citation: Bleicher, C., Qaralleh, A., Fliegener, S., Sommer, S., Kleinhans, R., Pintore, M., N., Study of the influence of recycling aluminum on the cyclic material behavior for chill cast AlSi7Mg0.3, Fracture and Structural Integrity, 77 (2026) 265-280.

Received: 28.02.2026
Accepted: 22.04.2026
Published: 06.05.2026
Issue: 07.2026

Based on alloy AlSi7Mg0.3 used in gravity die casting for car body components, three configurations — one primary alloy and two with accompanying elements — were cast and investigated through strain and stress-controlled tests. Results showed that additions of Fe and Zn lead to slightly increased cyclic and quasi-static material strength, whereas ductility was reduced.

KEYWORDS. Fatigue, Recycling, Aluminum, Chill casting, Gravity die casting, Cyclic loading.

INTRODUCTION

The future of vehicle construction is undergoing a major transformation towards more efficient production methods. A key development is "Giga-Casting" – a new car body construction method based on large integrated castings. This approach can drastically reduce production times, decrease dependency on supply chains, and save manufacturing steps and machinery.

At the same time, the automotive industry must achieve sustainability to meet climate targets while remaining socially fair, environmentally responsible, and cost-efficient. This requires reducing CO_2 emissions across all phases: material sourcing, production, and component use. Material optimization and lightweight design help save both resources and fuel.

The research project "FutureCarProduction" addresses these challenges. Its goal is to develop holistic solutions for evaluating new car body concepts. The project compares conventional processing, Giga-Casting, and new methods in terms of sustainability, technical performance, costs, and resource efficiency. It also investigates the use of recycled aluminum alloys – specifically the gravity die casting alloy AlSi7Mg0.3. Three variants are tested: a primary alloy and two recycled alloys with higher levels of iron (Fe), manganese (Mn), zinc (Zn), and copper (Cu). This paper focuses on the quasi-static and cyclic material behavior of these alloys.

STATE-OF-THE-ART

The cyclic material behavior of aluminum silicon alloys in cast components has been investigated within different research activities. In all of those investigations no focus was placed on the influence of the recycling material or additions of chemical elements like Cu or Zn that gather in the alloy during the recycling process. Nonetheless, several papers address the fatigue of AlSi alloys.

In [1] AlSi8Mg-T6 was detailed investigated for cast components with regard to microstructural effects. Nonetheless, no detailed fatigue data were derived and only under stress-control. Some further fatigue data for a primary alloy AlSi7Mg is provided by [2] with regard to the influence of material defects. In [3] Oberreiter et al. conducted and published a wide investigation on the fatigue of AlSi8Cu with regard to its cyclic stress- and strain-behavior as well as with regard to residual stresses and defects. The authors also discuss a layer model to transfer the derived data to a component level based on a fatigue assessment concept. This did not include an assessment of notch influences and a variation from primary to secondary alloys.

Further extensive evaluations of the fatigue life of cast aluminum alloys were done in [4] also for AlSi7Mg0,3 and AlSi8Cu3. Here the authors discuss the influence of mean loads and give an overview about results under stress-control for the application in the assessment process of cast components for gravity die casting as well as for high pressure die casting. Also, the influence of elevated temperatures and casting skins are determined. The results in [4] showed e.g. a wide range of mean stress sensitivities for all aluminum alloys from M = 0.13 to 0.60. A variation of the chemical composition to account for an influence coming from recycling effects did not take place, as well.

Further research on the fatigue of AlSi7 for cast components were carried out by [5], [6], [7], [8], [9] and [10]. Across all of these publications, the cyclic material behavior was examined exclusively in primary alloys, predominantly under stress-controlled conditions.

MATERIALS AND SAMPLING OF THE SPECIMENS

For the investigation the alloy AlSi7Mg0.3 cast in a gravity casting process in a chill mold was inspected since this process is commonly used to fabricate structural components for chassis applications. AlSi7Mg0.3 is known for its good mechanical and casting properties and are frequently joined to wrought materials through welding techniques to create robust sub-frames.
An investigation about the typical composition of the scrap and based on literature Fe and Cu are listed as problematic for the gravity casting process, since both elements influence the properties of aluminum alloys. Moreover, Mn and Zn are also determined as critical, [11][12]. With this information an experimental plan with three different alloys based on AlSi7Mg0.3 was developed to conduct a sensitivity analysis to simulate the accumulation of these elements and their influence on technological properties, Tab. 1. Tab. 1 also includes the chemical composition of the melts for the three alloys.

alloy	Chemical composition of the melts in [%]								Demand for samples				
	Si	Fe	Cu	Mn	Mg	Zn	Ti	Sr	static tensile	fatigue	hardness	microscopy	castings
S1: AlSi7Mg0.3 primary	6.90	0.106	0.003	0.042	0.287	0.006	0.145	0.022	16	68	4	8	**50**
S2: AlSi7Mg0.3 + Fe0.5 + Mn0.25	6.72	0.47	0.003	0.243	0.277	0.005	0.139	0.017	16	68	4	8	**50**
S3: AlSi7Mg0.3 + Fe0.5 + Mn0.25 + Cu0.35 + Zn0.2	6.82	0.487	0.338	0.242	0.272	0.196	0.142	0.018	16	68	4	8	**50**

Table 1: Design of experiment for the investigation of the influence of Fe, Mn, Cu and Zn on the performance parameters of AlSi7Mg0.3.

For each configuration, 42 samples were cast using gravity die casting. Fig. 1 shows the cast sample after the casting process with the removal position for the tensile, fatigue, hardness and metallographic specimens. All these samples were in the T6 heat treated with the following parameters: solution annealing temperature of ϑ = 535 °C for 260 min. The quenching followed in water at ϑ = 60 °C +/-3 °C with an artificial aging at ϑ = 165 °C for 150 min.

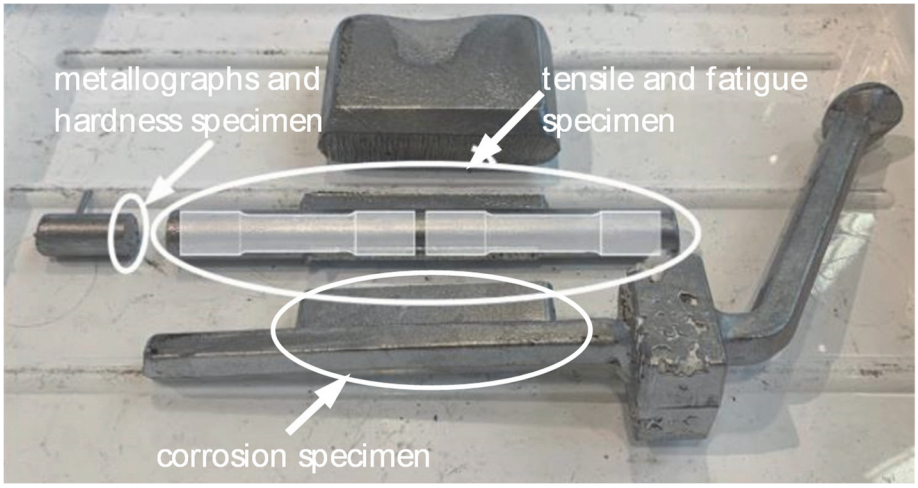

Figure 1: Removal position of the cast sample with two specimens for fatigue or tensile parameter characterization as well as for metallographic and hardness investigations.

Tab. 2 shows etched sections of each of the three material configurations. In S3 unwanted phases, such as β-Al5FeSi, can be found, which are known to slightly increase strength but significantly decrease ductility. No copper phases could be detected by EDX in the copper- and zinc-containing S2 and S3 variants, as it can be assumed that the copper and zinc accumulate in the mixed crystal. This hypothesis is also consistent with earlier work. The secondary dendrite arm spacing

was measured, too. In the mean values of 27 to 31 µm for the secondary dendrite arm spacing were measured. The difference between the different alloys was too little to be significant.
Besides the etched sections, hardness measurements were also conducted to evaluate the influence of the different alloying elements. The results are summarized in Fig. 2 and reveal the highest hardness values for S3 due to the addition of copper and zinc. The primary alloy S1 and the secondary alloy S2 showed in the maximum comparable hardness values of around 104 HV30 while S3 reached in the maximum a value of 108.2 HV30. Nonetheless, the scatter of the measured hardness is higher for S1 and S2 in comparison to S3.
Bevor the manufacturing of tensile and fatigue specimens started the round samples were inspected with X-ray computer tomography with Micro-CT setup, at 225 kV voltage and a voxel size of 100 µm. The volume of each individual pore was measured. For the characterization, only pores with equivalent ball diameter of 200 µm or above were taken into account for a later evaluation. The samples showed a good quality, and most specimens (> 80%) could be considered as sound and were used for the further evaluation process. Nevertheless, some samples showed small pores, Fig. 3, which were rejected from further investigation.

Etched sections to the materials investigated
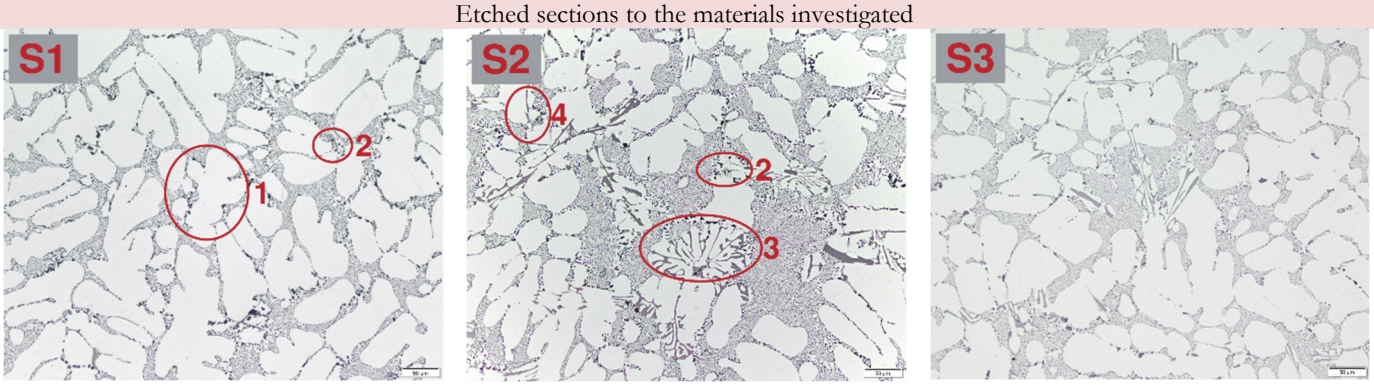
1: Alpha-solid solution dendrites; Eutectic in-between 2: Primary silicon precipitates and Mg2Si phases at the boundaries of the dendrites 3: Alpha-Al(Fe,Mn)Si phases 4: Beta-Al5FeSi precipitates (needle-shaped)

Table 2: Etched sections of the three configurations of the AlSi7Mg0.3

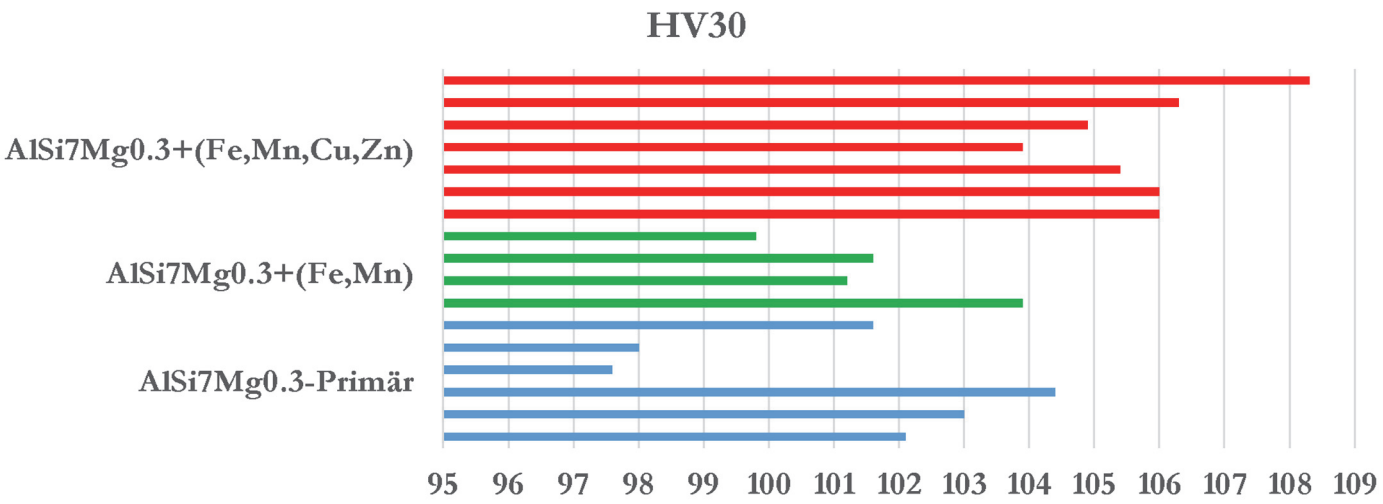

Figure 2: Results of hardness measurements according to Vickers (HV30).

From the sound samples two types of tensile specimens as well as several geometries as fatigue specimens for strain- and stress-controlled fatigue tests were manufactured. For the tensile tests two different specimen sizes with a test diameter of d = 6 mm and d = 10 mm were removed to investigate the influence of the size on the resulting tensile test parameters by 8 specimens for each size, Fig. 5. With regard to the latter application for the fatigue assessment of components for automotive industry the specimens with notches were designed with two different notch geometries: one with a mild notch

(K_t = 1.72) and another with a sharper notch (K_t = 2.50), Fig. 4. For each alloy 12 unnotched specimens were tested under strain control and 15 unnotched specimens for R_σ = -1 and R_σ = 0 each. From the samples 13 specimens were manufactured and tested under R_σ = -1 for each of the two notched specimens with K_t = 1.72 and K_t = 2.50.

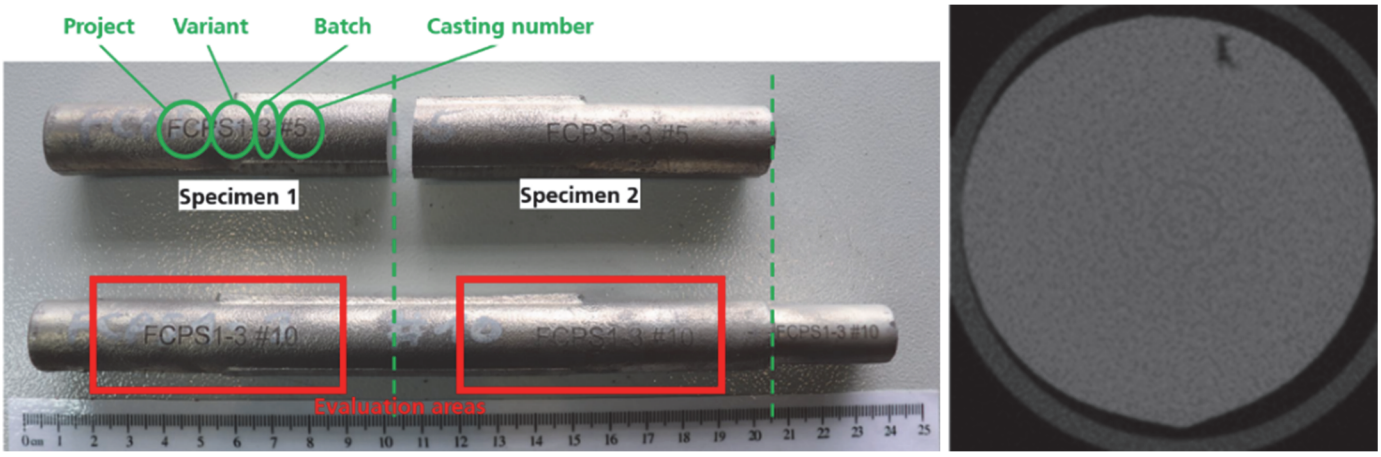

Figure 3: Left: Specimen removal from the casting, right: two exemplary results of the X-ray tomography inspection.

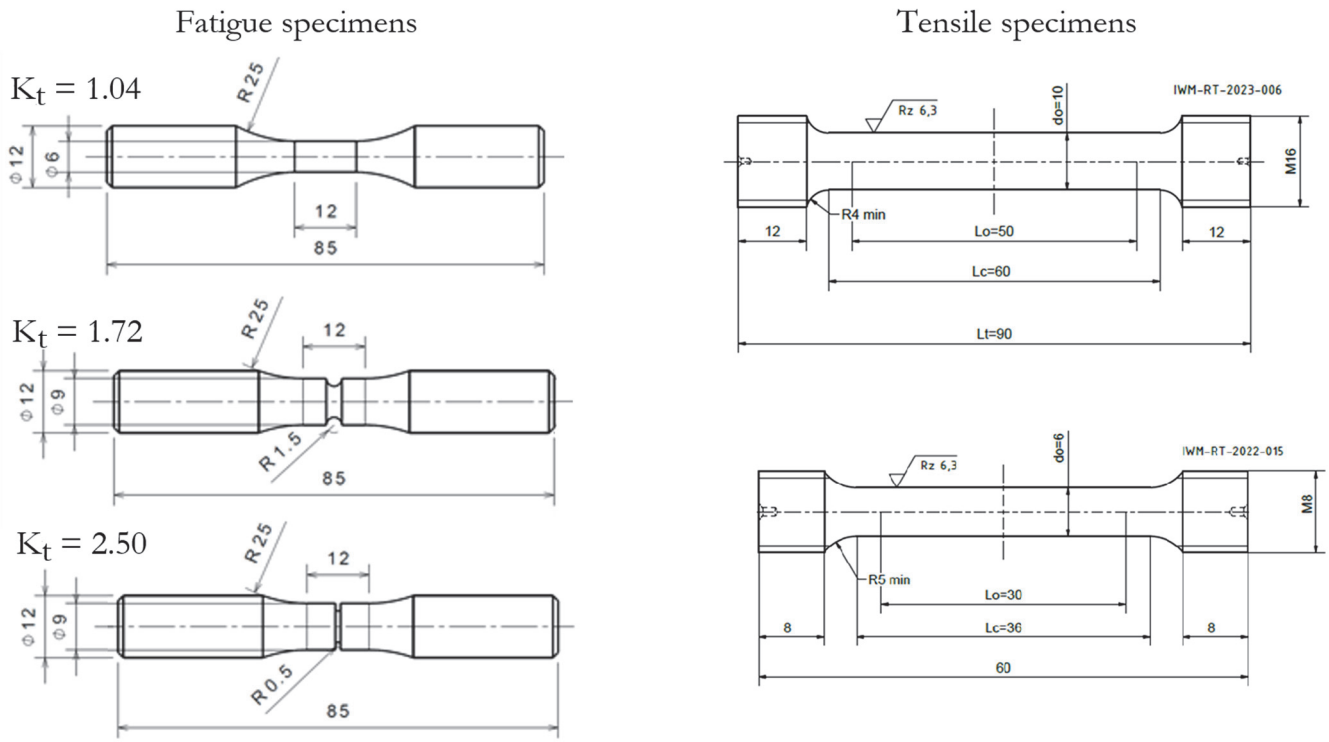

Figure 4: Tensile and fatigue specimens used for the investigations

QUASI-STATIC MATERIAL BEHAVIOR

The resulting tensile test parameters for both specimen configurations are given in Tab. 3. The results show that the addition of Fe, Mn (S2) slightly reduces $R_{p0.2}$ and R_m. In contrast to that, additions of Fe, Mn, Cu, Zn (S3) raise these parameters again slightly over the levels of the primary alloy of AlSi7Mg0.3 (S1). In general, however, yield stress $R_{p0.2}$ and tensile stress R_m are only slightly affected for the alloys S2 and S3, and the scatter within the test series is small. In contrast to this, elongation at fracture A_5 is strongly influenced by the alloying elements and the ductility highly reduced. Elongation at fracture A_5 is reduced from about 12% to 6% by adding Fe, Mn (S2) and even further reduced to about 3-

5% by adding Fe, Mn, Cu, Zn (S3). The reason for the observed differences in ductility are most likely influenced of the needle-like, intermetallic phases of iron in the microstructure, which are known to have negative effects on ductility and castability, Tab. 2. The comparison of the tensile test results for the two different specimens' sizes revealed no additional influence for the alloys S1 and S2. So, there is no additional statistical or geometrical size effect [13] within the three different alloys S1 and S2 under quasi-static loading. With regard to the alloy S3 the size effect is truly present when it comes to the tensile strength R_m and the elongation A_5. Here, both values are increased for the larger specimens. This is an unusual result. Mostly the fatigue and quasi-static data decrease with increasing specimen size due to the statistical and geometrical size effects [13]. A detailed view on the scatter band of the tensile test results showed a comparably high standard deviation for the primary material S1 with σ = 1.8 to 3.3. The other materials show a much smaller scatter in the range of σ = 0.6 to 1.1. All single tensile test results are summarized in Tab. 3.

Alloy	d [mm]	$R_{p0.2}$ [MPa]	R_m [MPa]	A_5 [%]	Alloy	d [mm]	$R_{p0.2}$ [MPa]	R_m [MPa]	A_5 [%]
S1	6	205.2	284.1	8.4	S1	10	213.9	295.8	13.6
S1	6	205.1	294.4	15.2	S1	10	214.5	297.2	12.9
S1	6	207.9	294.6	14.3	S1	10	205.9	294.0	14.4
S1	6	208.2	291.6	9.7	S1	10	210.7	293.2	10.1
Mean values		*206.6*	*291.2*	*11.9*	*Mean values*		*211.3*	*295.5*	*12.8*
S2	6	199.7	271.6	6.4	S2	10	206.9	275.8	6.5
S2	6	206.6	276.7	6.2	S2	10	205.3	273.2	5.3
S2	6	203.1	273.1	6.0	S2	10	211.7	277.6	5.5
S2	6	206.9	270.3	5.0	S2	10	208.8	276.3	6.2
Mean values		*204.1*	*272.9*	*5.9*	*Mean values*		*208.2*	*275.7*	*5.9*
S3	6	222.5	287.0	3.8	S3	10	222.4	292.2	5.4
S3	6	226.2	287.1	3.3	S3	10	219.7	290.4	5.2
S3	6	221.6	277.6	2.5	S3	10	220.4	291.7	5.2
S3	6	223.8	264.9	1.3	S3	10	218.5	284.0	3.9
Mean values		*223.5*	*279.2*	*2.7*	*Mean values*		*220.3*	*289.6*	*4.9*

Table 3: Results of the tensile tests with regard to the two different specimen diameters

FATIGUE TESTING

To derive an entire overview about the cyclic material behavior of the influence of secondary aluminum both stress- and also strain-controlled fatigue tests were performed. This incorporates the fatigue assessment of unnotched specimens with load ratios of R_σ = -1 and R_σ = 0 under stress-controlled to assess the mean stress sensitivity and the influence of notches based on two different notched specimens.

The fatigue tests will be conducted using a resonance test machine with a maximum load capacity of 20 kN and a test frequency of up to f = 150 Hz. All specimens were axially loaded with a sinusoidal signal at room temperature and until the final failure or until reaching the limit number of cycles of $N_{lim} = 1 \cdot 10^7$.

The statistical evaluation was conducted based on the maximum likelihood method according to Spindel and Haibach [14] and Stoerzel [15] to derive the SN curve parameters for a probability of survival of P_S = 10%, 50% and 90%. Furthermore, the scatter band Tσ and the slope of the SN curve k was determined. The slope after the knee point N_k was assumed to be k* = 22, which corresponds to a decrease in fatigue strength of 10 % per decade according to Sonsino [16].

The strain-controlled fatigue tests were performed under sinusoidal loading with constant amplitude on servo-hydraulic test rigs. For applying the strain, an extensometer with a maximum gauge length of 10 mm was used. The investigations were done in accordance to [17]. This guideline provides information about test frequencies in relation to the applied total strain $\varepsilon_{a,t}$, fatigue specimen geometries, test conditions, and the final evaluation of the results. The fatigue tests were performed until crack initiation or until the limit number of cycles $N_{lim} = 1 \cdot 10^7$. In this test series, specimens were tested in the frequency range of f = 0.1 and 10 Hz. From the fatigue tests, the strain-life curve according to Coffin [18], Manson [19], Basquin [20], and Morrow [21] was determined.

The cyclic stress–strain response was derived from stabilized hysteresis loops obtained under strain-controlled fatigue loading. All investigated alloys exhibit a nonlinear elastic–plastic behavior, which can be described using a Ramberg–Osgood relationship as in Eqn. (1):

$$\varepsilon_a = \frac{\sigma_a}{E} + \left(\frac{\sigma}{K'}\right)^{\frac{1}{n'}} \quad (1)$$

where ε_a is the strain amplitude, σ_a is the stress amplitude, E the Young's modulus, and K' and n' the cyclic strength coefficient and cyclic strain hardening exponent, respectively. Moreover, the strain–life diagrams are plotted based on the Coffin–Manson-Basquin-Morrow relationship given in Eqn. (2).

$$\varepsilon_a = \varepsilon_{a,elastic} + \varepsilon_{a,plastic} = \frac{\sigma_f'}{E}\left(2N_f\right)^b + \varepsilon_f'\left(2N_f\right)^c \quad (2)$$

where σ'_f is the fatigue strength coefficient, ε'_f is the fatigue ductility coefficient, and both b and c are the fatigue strength exponent and fatigue ductility exponent, respectively.
For the calculation of the strain-life and the cyclic stress-strain curve parameters (Eqs. 1 and 2) according to SEP1240 [17] the elastic strain $\varepsilon_{a,e}$ is first calculated by dividing the stress amplitude σ_a by the Young's modulus E. The Young's modulus E is determined from the strain-controlled fatigue tests for each material. To derive the plastic fraction of the total strain, the calculated elastic strain $\varepsilon_{a,e}$ is subtracted from the measured total strain $\varepsilon_{a,t}$.
By plotting and linear regression through the elastic and plastic fractions of each strain-controlled fatigue test, one is able to calculate the strain-life curve parameters Eqn. (2).
Additionally, the parameters for the trilinear strain-life curve according to Wagener [22] were determined. In the trilinear approach the elastic strain-life curve Eqn. (2) is divided into three parts: one for the low cycle, one for the medium cycle, and one for the very high cycle lifetime regime. This approach corresponds then to the behavior of the stress life curve in which the medium cycle and the high cycle fatigue regime are separated by a knee point. The advantage of the trilinear approach is that fatigue results are much better met and that the method enables the definition of a knee point according to stress-life curves. A detailed description of the evaluation process for cast materials can be found in Bleicher [23].

CYCLIC MATERIAL BEHAVIOR UNDER STRESS CONTROL

Fig. 5 and Fig. 6 show the results of the stress-controlled fatigue tests on the unnotched and notched specimens under alternating and tensile loading. The results on the unnotched specimens, Fig. 5, show that the primary alloy (S1) has the steepest slope k in the medium cycle regime so before the knee point N_k. The knee point itself differs strongly between the different alloys under alternating loading. For the high cycle fatigue regime results under alternating loading, R_σ = -1, all alloys achieved a comparable nominal stress amplitude $\sigma_{a,n}$ of 105 MPa (S1 and S3) and 106 MPa for S2. Concerning the relation of the slopes k the three alloys show a comparable behavior under tensile loading, R_σ = 0. An improvement was determined for the high cycle fatigue regime: Here, the secondary alloys show a somewhat higher fatigue strength ($\sigma_{a,n}$ = 74 MPa for S2 and $\sigma_{a,n}$ = 72 MPa for S3) than the primary alloy (S1, $\sigma_{a,n}$ = 65 MPa). A comparison to literature data for the results under alternating loading shows that the determined values even exceed data from AlSi8Cu3-T6 alloy [3] which were achieved ($\sigma_{a,n}$ = 62.8 MPa) by a vibratory finished post treatment of the specimens. Moreover, this AlSi8Cu3-T6 alloy has with 7.5 to 8.5 % a by around 2 % higher silicon content as the investigated alloys S1, S2 and S3. Also, the Cu, Mn and Ti content are higher in [3]. A companion to findings in [4] for a primary AlSi7Mg0.3 shows that the current investigation meets the by Qaralleh derived results very well.
The lifetime assessment of cast components is usually driven by load ratios that are not equal to -1 or 0. For these cases it is necessary to assess the mean stress sensitivity for the different alloys. The mean stress sensitivity M for S1 at N_{lim} is 0.62 which is comparably high with regard to the secondary alloys S2 (M = 0.43) and S3 (M = 0.46). Results from these investigations are in good agreement with results for the same alloy as a primary material investigated in [4] for gravity die casting.
For the fatigue tests on the notched specimens the SN curves for all three alloys show comparable results. This makes even more sense since notches are equalizers for fatigue strength. The only difference occurs for the results under alternating loading in the high cycle fatigue regime. Here the alloys S2 and S3 show an around 13 MPa higher fatigue strength for K_t = 1.72 specimens compared to S1. This difference vanishes completely for the sharper notches (K_t = 2.50).

For the fatigue evaluation and safety assessment of automotive components the scatter band plays an important role. With increasing scatter bands of the material in stress direction the safety factor needs to be increased likewise to prevent the component not failing during usage. But safety can only be increased by reducing the stress level on the component meaning by increasing the wall thickness of components. This implies that the lightweight potential decreases. With this regard it is most favorable to achieve a material with a small scatter band.

For the three alloys S1, S2 and S3 the scatter band T_σ did not show a clear tendency. While alloy S2 reached comparable narrow scatter bands of T_σ = 1:1.20 the primary alloy S1 exceeded a typical value for cast material of T_σ = 1:1.30 that Bleicher [25] recommends for the design of cast components by far. Under alternating loading S1 showed a scatter band of T_σ = 1:1.36 and under tensile loading T_σ = 1:1.46. Also, S3 reached with T_σ = 1:1.38 a high scatter band. Typically, higher scatter bands are based on problems with the presence of defects like shrinkages or pores, [25]. Nonetheless, based on the results of the quality assurance process none of those defects have led to such a scatter band. Thus, it must be stated that the derived scatter bands are implications of the alloy's microstructure itself.

The influence of the microstructure of the three different alloys on fatigue cannot clearly be stated since the differences are comparably low and not directionally stable. For the notched conditions with K_t = 2.50 the microstructural influence vanishes completely. For the specimens with K_t = 1.72 and the unnotched specimens under R_σ = 0 for S2 and S3 reveal no difference between each other but clearly against S1. So, the additions of Fe and Mn increase the fatigue strength while Cu and Zn achieve no further contribution to an enhanced fatigue performance. Although a lot of irregularities were found in S2 and S3 (Tab. 2) with Mg2Si phases at the boundaries of the dendrites, Alpha-Al(Fe,Mn)Si phases and Beta-Al5FeSi precipitates the overall fatigue performance is positive with regard to S1. This result is even more impressive since the scatter band of the fatigue results for S2 and S3 is much better compared to S1.

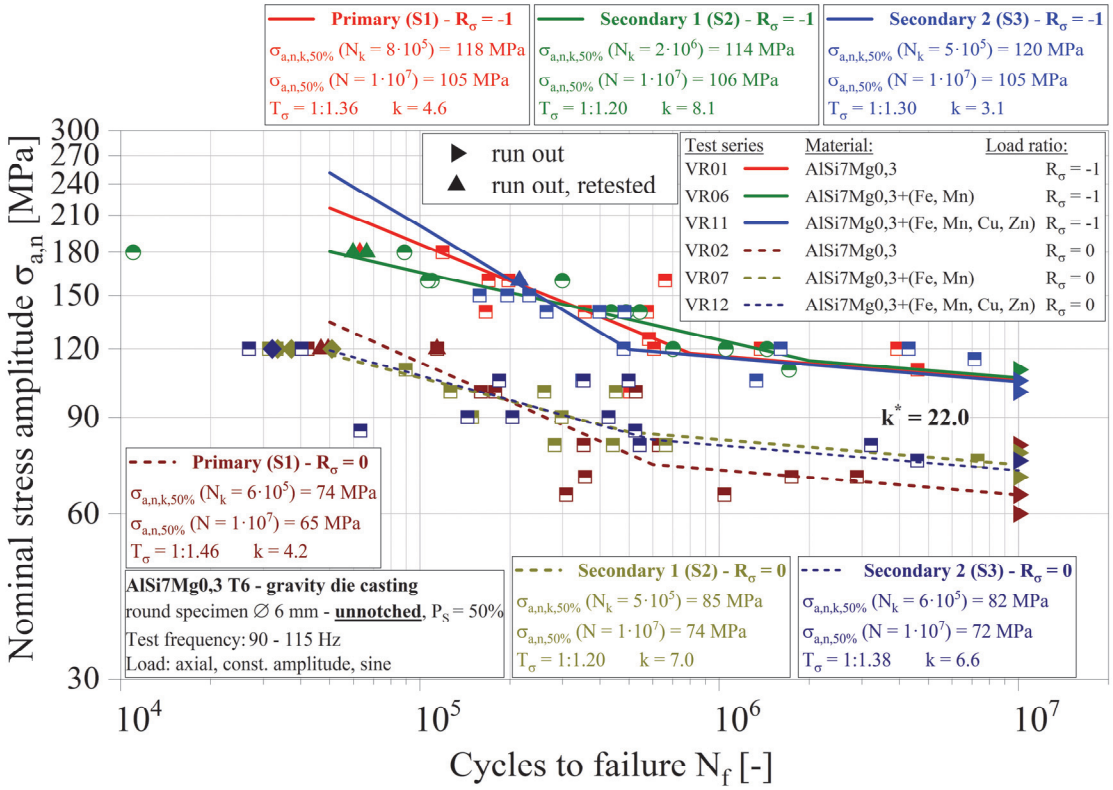

Figure 5: Comparison of the stress-life curves for the three different alloys for alternating, R_σ = -1, and tensile loading, R_σ = 0, derived for unnotched specimens [24].

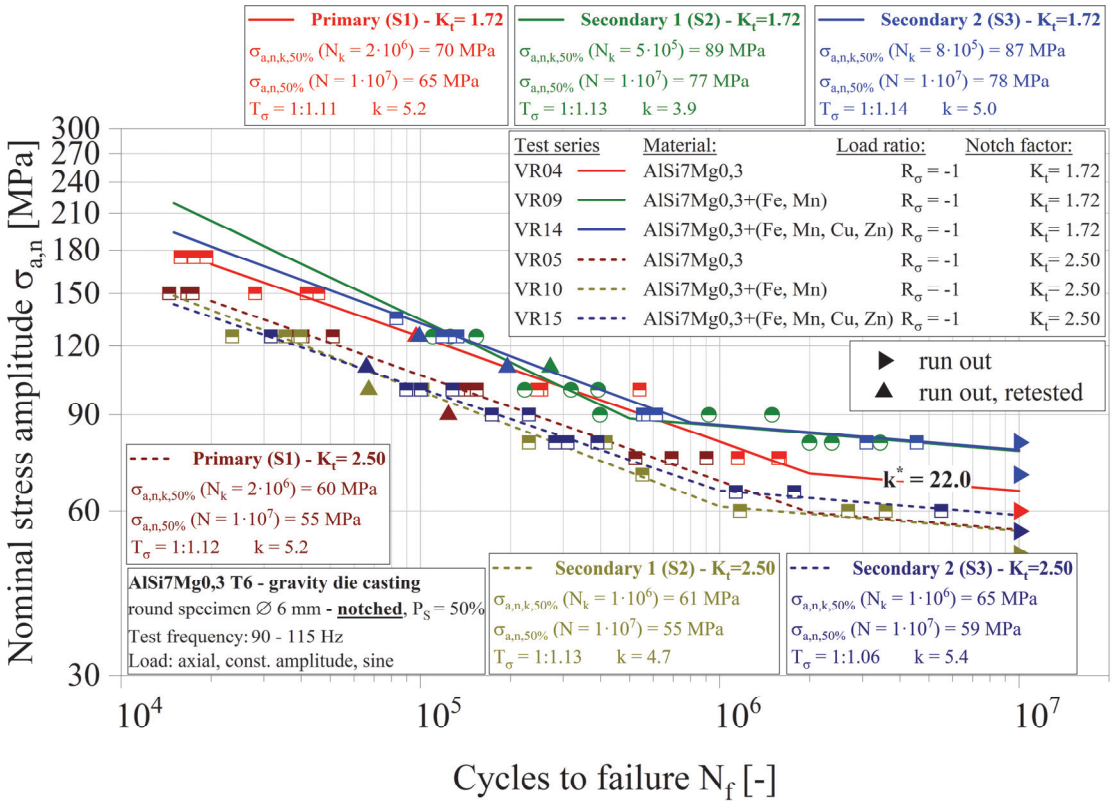

Figure 6: Comparison of the stress-life curves for the three different alloys for alternating loading, R_σ = -1, derived for notched specimens [24].

CYCLIC MATERIAL BEHAVIOR UNDER STRAIN CONTROL

Fig. 7 shows the determined cyclic stress–strain curves for the investigated aluminum alloy AlSi7Mg0.3, including the primary alloy and the two secondary alloys S2 and S3, as well as their direct comparison. The cyclic stress–strain curves of all investigated alloys exhibit pronounced cyclic hardening behavior. Furthermore, as can be seen in the lower-left diagram of Fig. 7, the secondary alloy variant S2 shows a significantly lower resistance to cyclic deformation beyond the cyclic yield point, along with a noticeably higher scatter compared to S1 and S3. In contrast, S1 and S3 display nearly identical cyclic material behavior. However, S3 is characterized by a slightly higher cyclic yield strength of approximately 302 MPa, and the difference relative to the primary alloy S1 decreases at higher strain amplitudes.

Fig. 8 to 11 depict the strain-life curves for the three materials. This shows clearly that the primary alloy (S1) exhibits the highest fatigue resistance in the low-cycle fatigue (LCF) regime, where plastic strain dominates. This behavior persists up to approximately $N = 1 \cdot 10^5$ cycles, beyond which the differences between the materials gradually diminish. In the very-high-cycle fatigue (VHCF) regime, where elastic strain dominates, it is noticeable that S2 exhibits a slightly higher fatigue strength compared to S1 and S3. This indicates that, for applications in which severe plastic deformation is expected, the primary alloy represents the more suitable material choice. The secondary alloys reveal a reduction in fatigue life, particularly at higher strain amplitudes.

A key aspect of the present evaluation is the application of a trilinear approximation of the strain–life curve instead of the conventional bilinear representation. The trilinear approach enables a more accurate description of the transition between the low-cycle fatigue (LCF) and high-cycle fatigue (HCF) regimes by introducing an additional change in slope und thus a knee point in the medium fatigue range towards the high cycle fatigue range. This enables a direct comparison in the description of the strain-life curve to the stress-life curve. Using a trilinear approach is particularly beneficial for aluminum cast alloys, which was first described by Wagener [22] for aluminum materials.

Overall, the combined evaluation of cyclic stress–strain behavior and strain–life curves demonstrates that the use of secondary aluminum alloys can represent a sustainable and, in some cases, beneficial option for structural components, as they may exhibit comparable or even superior mechanical properties to primary alloys in terms of cyclic deformation

resistance and fatigue lifetime. However, the extent to which secondary alloys can be applied strongly depends on the specific loading conditions and application requirements, as well as on the quality and microstructural condition of the secondary material, as evidenced by the differences observed among the investigated secondary alloys.

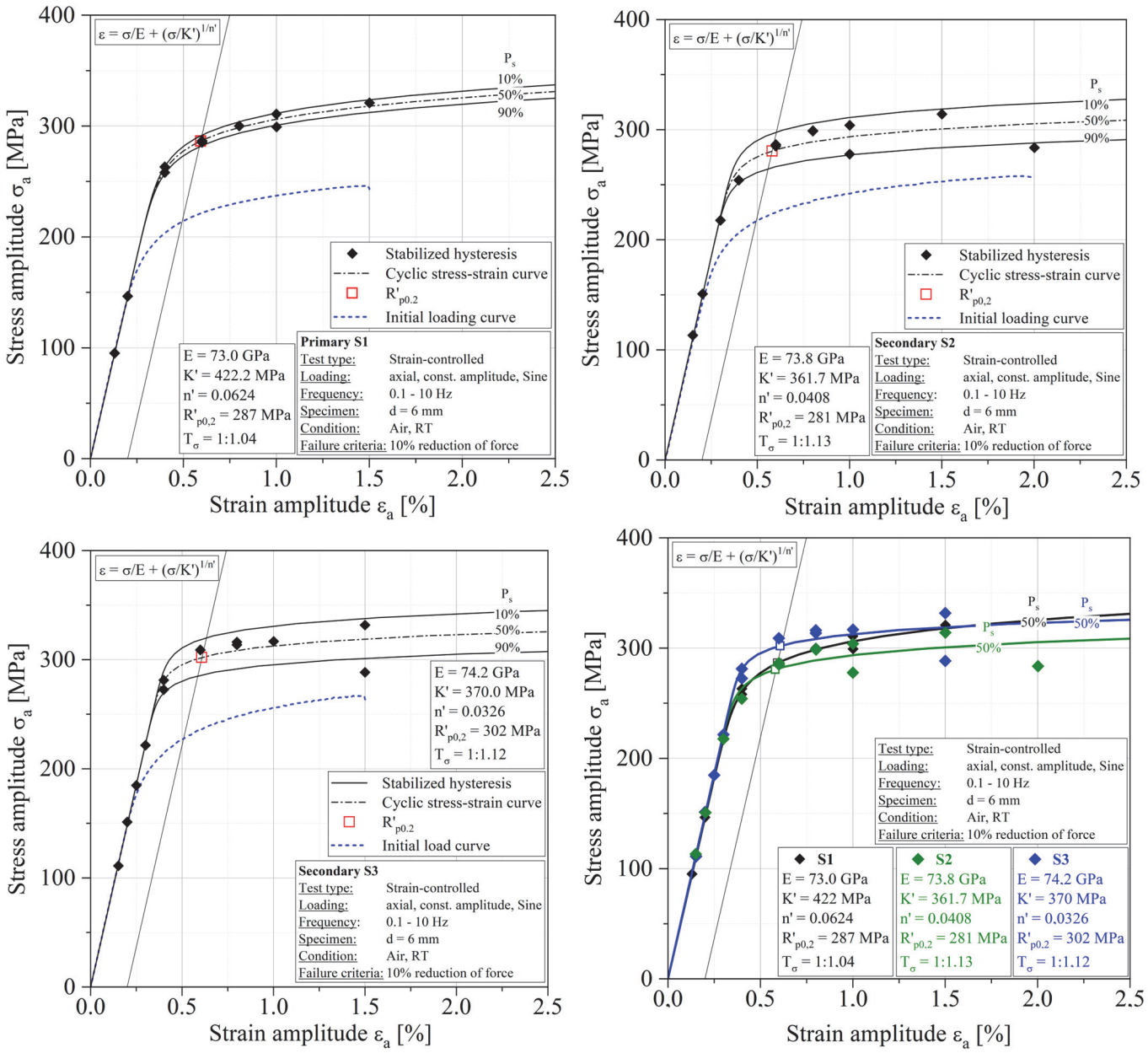

Figure 7: Upper, left: Cyclic stress-strain curves for the primary alloy S1; upper, right: Cyclic stress-strain curves for the secondary alloy S2; lower, left: Cyclic stress-strain curves for the secondary alloy S3; lower, right: Comparison of all cyclic stress-strain curves.

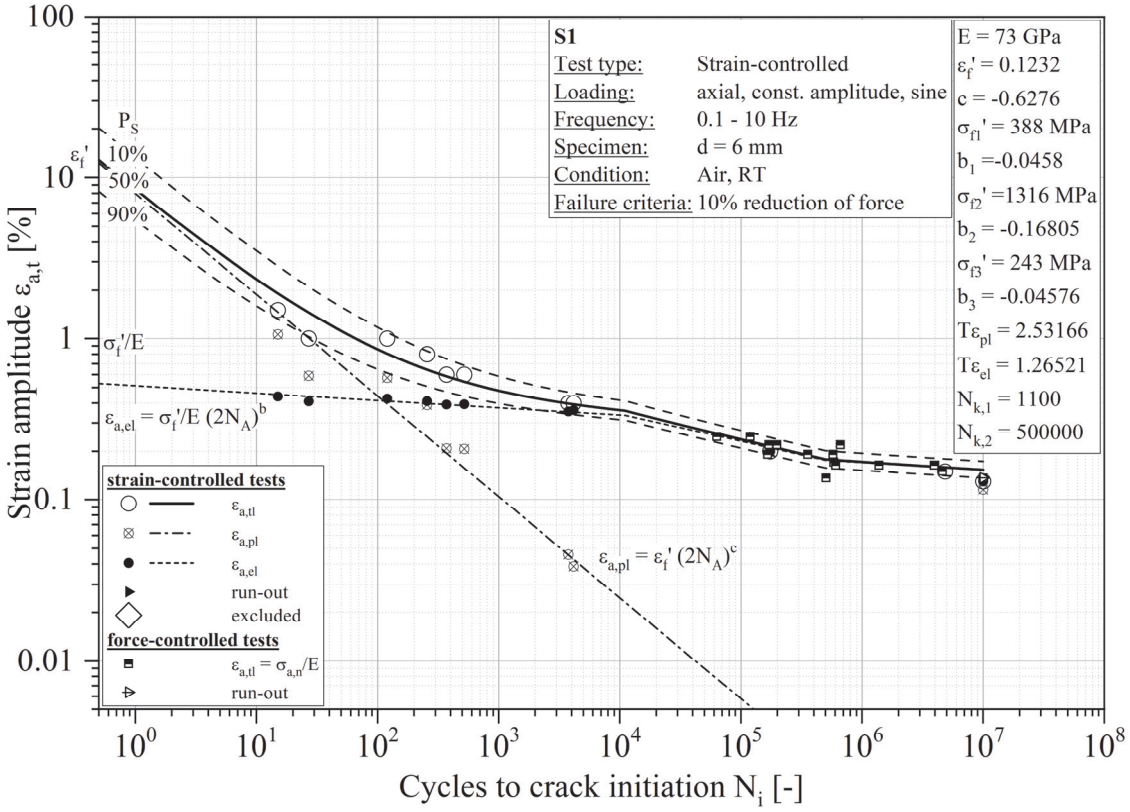

Figure 8: Strain-life curves for the primary alloy S1.

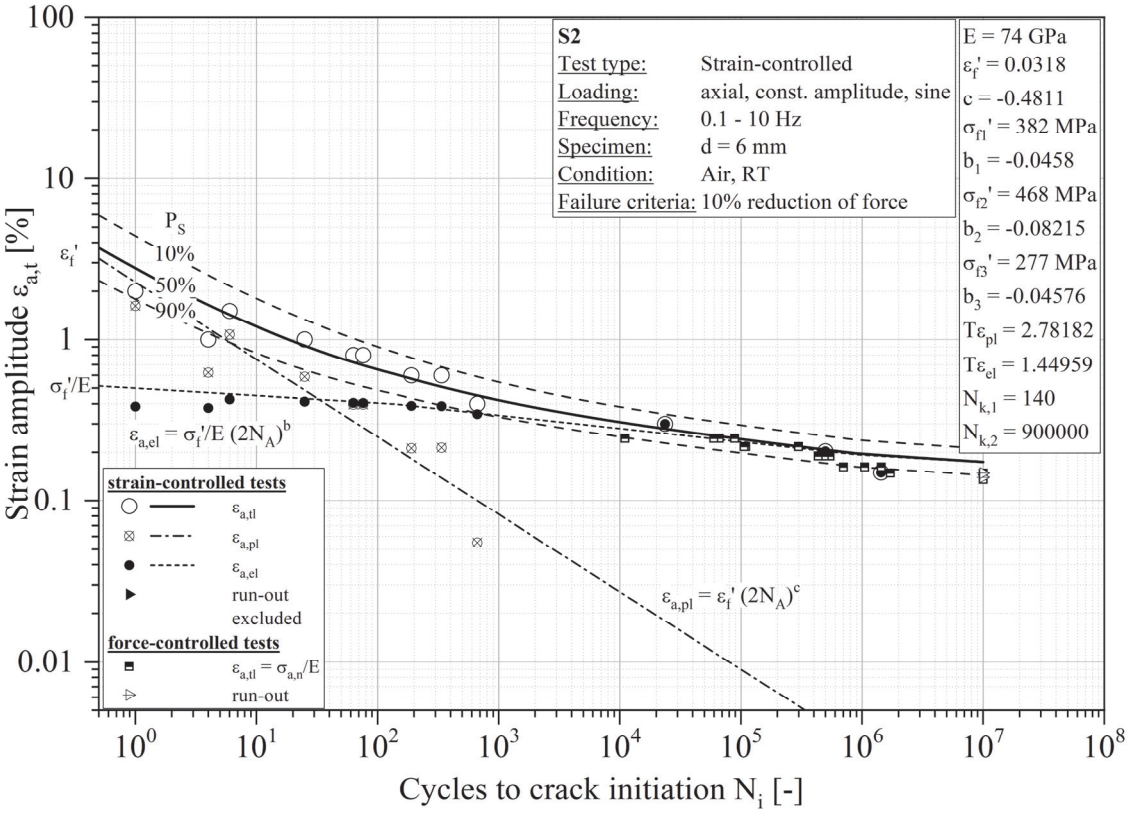

Figure 9: Strain-life curves for the secondary alloy S2.

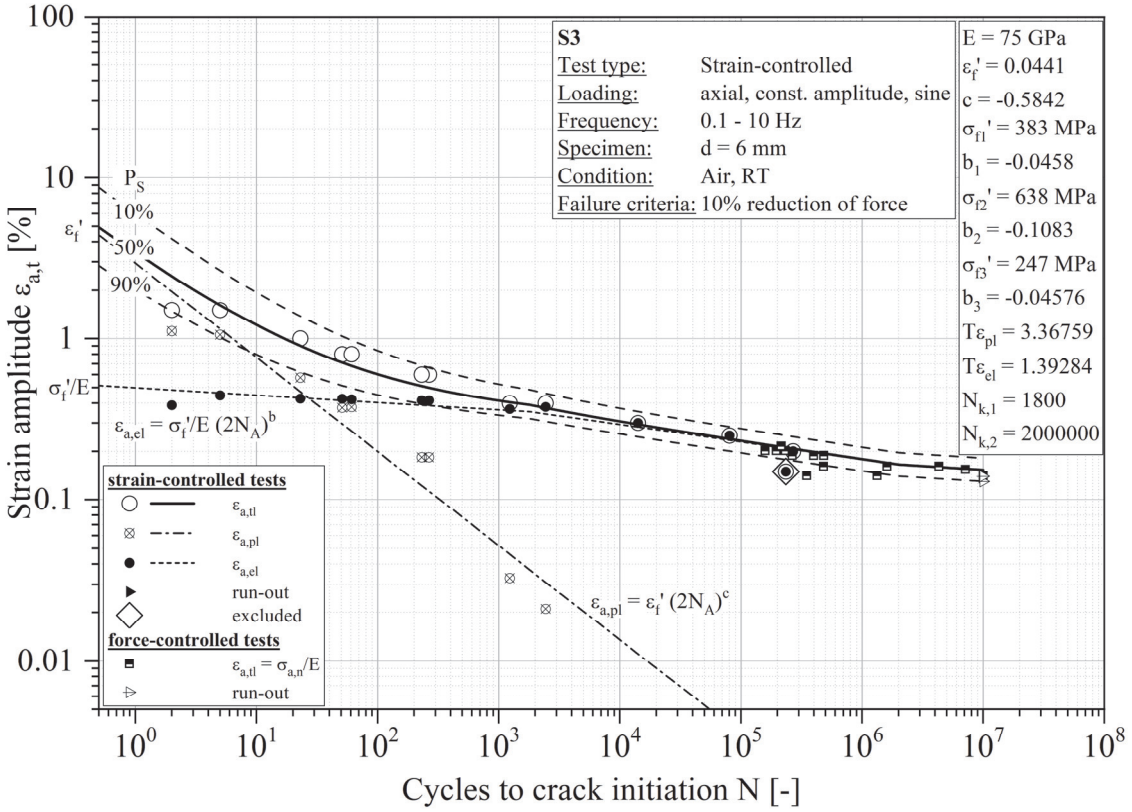

Figure 10: Strain-life curves for the secondary alloy S3.

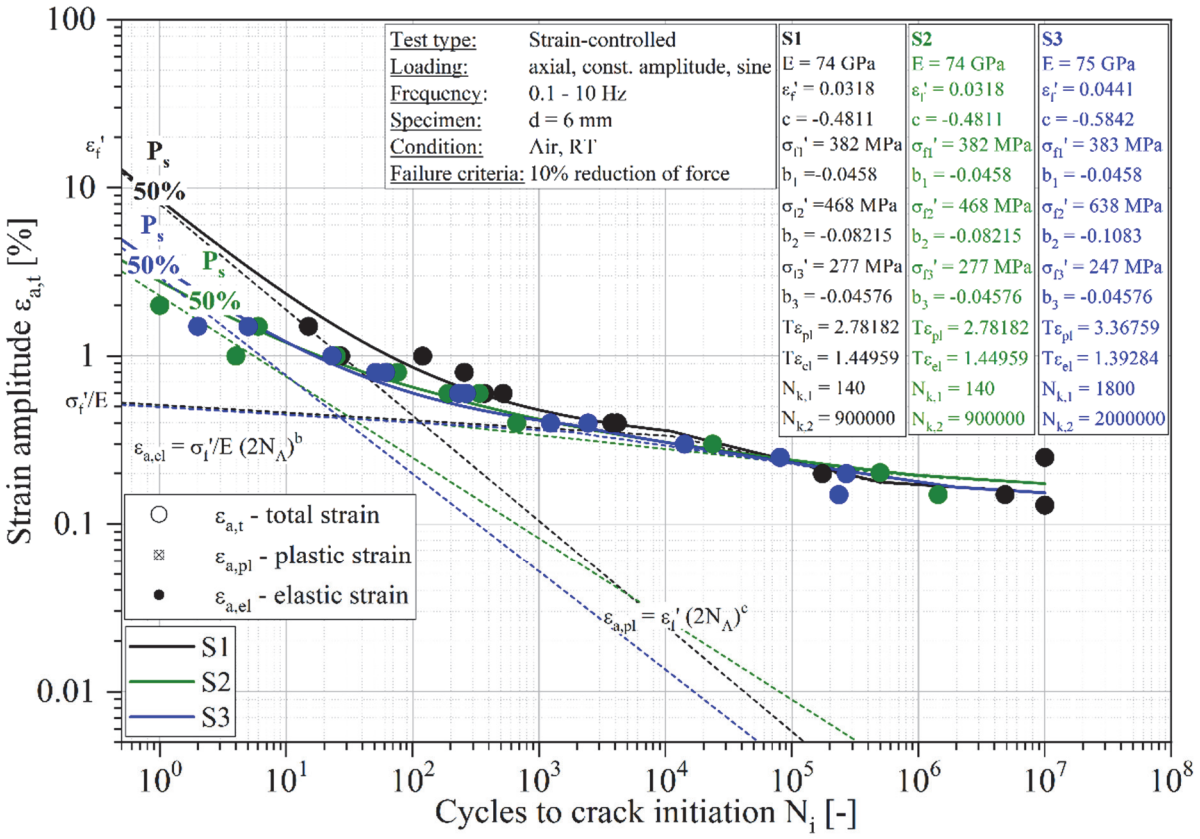

Figure 11: Comparison of all derived strain-life curves.

CONCLUSIONS AND OUTLOOK

This study investigates how increased recycling content in aluminum casting alloys affects quasi-static and cyclic material behavior. The gravity die casting alloy AlSi7Mg0.3 serves as the primary alloy and is tested in two additional configurations. Motivated by the automotive industry's need to reduce CO_2 emissions and support concepts such as "Giga-Casting," the work examines whether secondary aluminum alloys with higher levels of accompanying elements can maintain or improve mechanical performance while lowering the carbon footprint.

This paper provides an overview of the research project "FutureCarProduction" and its main objectives: evaluating sustainability, performance, and costs of modern car body production methods. Three alloy variants were produced using a chill-mold gravity casting process: a primary AlSi7Mg0.3 alloy (S1), a secondary alloy with added Fe and Mn (S2), and a further modified alloy with Fe, Mn, Cu, and Zn (S3).

Metallographic analysis showed comparable secondary dendrite arm spacings across all alloys. However, S3 contained needle-shaped β-Al_5FeSi phases, which are known to increase strength but reduce ductility. Hardness measurements revealed the highest values for S3, while S1 and S2 showed similar but more scattered results.

Quasi-static tensile tests showed that ductility was strongly affected by recycling content. The elongation at fracture (A5) dropped from approximately 12% in S1 to roughly 6% in S2 and 3–5% in S3, reflecting the detrimental effect of Fe-rich intermetallic phases.

To characterize cyclic behavior, both stress-controlled and strain-controlled fatigue tests were performed on unnotched and notched specimens under different load ratios. Stress-life (S–N) evaluations showed that secondary alloys do not suffer fatigue reductions. In the high-cycle regime under tensile loading, S2 and S3 even exhibited higher fatigue strength than S1 and showed reduced mean stress sensitivity. Strain-controlled fatigue tests revealed cyclic hardening in all alloys. The primary alloy S1 offered the best low-cycle fatigue performance, consistent with its higher ductility observed in tensile tests. S2 showed slightly improved behavior in the very-high-cycle regime, predominantly in the elastic range. The loss in ductility both of the quasi-static and cyclic material properties can limit the use of these materials in components, that are partly subjected to elasto-plastic material behavior or impacts or crash. This includes also load scenarios in which extreme loads or misuse are included that lead locally to elasto-plastic strains. In these cases, the alloys S2 and S3 are not as performaned as the primary alloy S1. Nonetheless, for a practical application in cases where no larger elasto-plastic strain occur the S2 and S3 alloys can considered to be better than the primary alloy. Especially when it comes to lightweight the S2 and S3 alloys achieve an improvement in the total mass for unnotched or only slightly notched components. This is the case not only based on the improved nominal stress amplitude but also on the reduced scatter band. In contrast to that the investigations revealed an unexpectedly high scatter band for the primary alloy S1 for unnotched specimens and a high mean stress sensitivity M. For an application in an automotive component the designer and structural durability expert have to decide component by component, if a primary or secondary alloy can be used and balance lightweight potential against the loss in ductility for components that might face extreme loads.

In summary, the investigations showed no significant negative influence on quasi-static and cyclic material properties for car body components made of AlSi7Mg by low-pressure die casting or gravity casting. Only ductility suffers from the additions of Fe, Cu, Mn, and Zn, as demonstrated by tensile tests and low-cycle fatigue results. All other investigated parameters benefited from the secondary alloys.

The study did not include fatigue testing under corrosive conditions such as salt spray. Under such conditions, a reduction in fatigue strength for S3 is likely due to its increased copper content, which promotes corrosion in aluminum alloys.

The research in "FutureCarProduction" extends beyond these chill castings of AlSi7Mg0.3. Future work will investigate high-pressure die cast alloys such as AlSi10MnMg to determine whether secondary alloys have positive or negative effects in those applications.

ACKNOWLEDGEMENTS

The results presented in this paper were derived during the research project “FutureCarProduction“. For the funding of this project, sincere thanks are given to the Fraunhofer Gesellschaft. We also want to thank our Fraunhofer colleagues for their contributions to the entire project.

NOMENCLATURE

A_5 [-]	Elongation at fracture
Al	Aluminum
b [-]	Fatigue strength exponent
c [-]	Fatigue ductility exponent
Cu	Copper
d [mm]	Diameter of the specimen
E [GPa]	Young's modulus
f	Test frequency
f [Hz]	Test frequency
Fe	Iron
k [-]	Slope of the SN curve in the medium cycle fatigue range
k* [-]	Slope of the SN curve after the knee point
K‘ [MPa]	Cyclic hardening coefficient
K_f [-]	Fatigue notch factor
K_t [-]	Stress concentration factor
M [-]	Mean stress sensitivity
Mn	Manganese
N [-]	Number of cycles
n‘ [-]	Cyclic hardening exponent
N_f [-]	Number of cycles to failure
Ni	Nickel
N_i [-]	Number of cycles to crack initiation
N_k	Number of load cycles at the knee point
N_k [-]	number of cycles at the knee point
N_{lim}	Limit number of cycles
N_{lim} [-]	limit number of cycles
P_S [%]	probability of survival
$R‘_{p0,2}$ [MPa]	cyclic yield strength
R_m	Tensile strength
$R_{p0.2}$	Yield strength
R_s	Load ratio under stress
R_ε, R_σ [-]	load ratio under constant amplitude loading for strain and stress
Sn	Tin
T_σ [-]	Scatter band in stress direction
$T_{\varepsilon,pl}$	Scatter band in strain direction for the plastic strain-life curve
$T_{\varepsilon,el}$	Scatter band in strain direction for the elastic strain-life curve
Zn	Zinc
ϑ [°C]	Temperature
ε'_f [m/m]	fatigue ductility coefficient
$\varepsilon_{a,e}$ [%]	elastic strain
$\varepsilon_{a,p}$ [%]	plastic strain
$\varepsilon_{a,t}$ [%]	total strain under constant amplitude loading
σ	standard deviation
σ'_f [MPa]	fatigue strength coefficient
$\sigma_{a,n,k}$ [MPa]	nominal stress amplitude at the knee point
$\sigma_{a,n,Nlim}$ [MPa]	Nominal stress amplitude at the limit number of cycles

REFERENCES

[1] Pavesi A., Bandiera M., Mancini A., Tsyupa B., Bonfanti A., Casari D., Barella S., D'Errico F., Bertasi F. (2023) Effect of anodizing on high cycle fatigue behaviour of cast AlSi8Mg-T6 alloy, International Journal of Fatigue, 176, 107836, DOI: https://doi.org/10.1016/j.ijfatigue.2023.107836

[2] Redik S., Tauscher M., Grün F. (2014). Mechanisms of fatigue-crack initiation and their impact on fatigue life of AlSi7 die-cast components, MATEC Web of Conferences, 12, 03003, DOI: https://doi.org/10.1051/matecconf/20141203003
[3] Oberreiter, M., Horvath, M., Stoschka, M., & Fladischer, S. (2023). Effect of Surface Finishing State on Fatigue Strength of Cast Aluminium and Steel Alloys. Materials, 16(13), 4755. DOI: https://doi.org/10.3390/ma16134755
[4] Qaralleh, A., Niewiadomski, J., Bleicher, C. (2025). Advanced Characterization of Mechanical and Cyclic Fatigue Properties of Aluminum Cast Materials for Optimized Industrial Applications, SAE Technical Papers, DOI: https://doi.org/10.4271/2025-01-8237
[5] Tenkamp J., Blinn B., Beck T., Walther F. (2023). Microstructure- and plasticity-based fatigue and defect tolerance assessment of agehardenable Al-Si cast alloys in LCF and HCF regime, International Journal of Fatigue, 166, 107240, DOI: https://doi.org/10.1016/j.ijfatigue.2022.107240
[6] Tenkamp, J., Awd, M., Siddique, S., Starke, P., & Walther, F. (2020). Fracture–Mechanical Assessment of the Effect of Defects on the Fatigue Lifetime and Limit in Cast and Additively Manufactured Aluminum–Silicon Alloys from HCF to VHCF Regime. Metals, 10(7), 943. DOI: https://doi.org/10.3390/met10070943
[7] Oberreiter, M., Pomberger, S., Leitner, M., & Stoschka, M. (2020). Validation Study on the Statistical Size Effect in Cast Aluminium. Metals, 10(6), 710. DOI: https://doi.org/10.3390/met10060710
[8] El Khoukhi, D., Morel, F., Saintier, N., Bellett, D., Osmond, P., Le, V.-D., Adrien, J., (2022). Scatter and size effect in High Cycle Fatigue of cast aluminum-silicon alloys: A comprehensive experimental investigation, Procedia Structural Integrity, 38, pp. 611-620, DOI: https://doi.org/10.1016/j.prostr.2022.03.063.
[9] Ren, P., Huang, W., Zuo, Z., Li, D., Zhao, C., Yan, K., (2022). High cycle fatigue analysis and modelling of cast Al–Si alloys extracted from cylinder heads considering microstructure characteristics, Journal of Materials Research and Technology, Volume 19, pp. 3004-3017, DOI: https://doi.org/10.1016/j.jmrt.2022.05.186.
[10] Li, H., Zhang, W., Yang, S., Cai, G., Wang, X., (2025). Study on the High-Cycle Fatigue and Fatigue Crack Growth Behavior of Al–Si–Mg Alloy: Pore Size and Stress Ratio Effects. Fatigue & Fracture of Engineering Materials & Structures, 48(8), pp. 3475-3486.
[11] Beyer, T., Kleinhans, R., Rosefort, M., Klan, S., Siemund, P., Decker, P., Volk, W. (2024). Influence of Increased Fe, Cu, and Zn Concentrations on Phase Formation in Aluminum A356 (AlSi7Mg0.3) Alloy, Light Metals, pp. 234 - 239, DOI: https://doi.org/10.1007/978-3-031-50308-5_29.
[12] Taylor, J. A. (2012). Iron-Containing Intermetallic Phases in Al-Si Based Casting Alloys, Procedia Materials Science 1, DOI: https://doi.org/10.1016/j.mspro.2012.06.004.
[13] Kloos K. H., Buch A., Zankov D. (1981). Pure geometrical size effect in fatigue tests with constant stress amplitude and in programme tests. Materialwissenschaft und Werkstofftechnik. 12(2), pp. 40–50, DOI: https://doi.org/10.1002/mawe.19810120205.
[14] Spindel, J, E, Haibach, E. (1979). The method of maximum likelihood applied to the statistical analysis of fatigue data including run-outs, S.E.E. International Conference, University of Warwick, Coventry, 3rd to 6th April, pp. 7.1 – 7.23.
[15] Stoerzel, K., Baumgartner, J. (2021). Statistical evaluation of fatigue tests using maximum likelihood, Materials Testing, De Gruyter, 63, 8, pp. 714 – 720, DOI: https://doi.org/10.1515/mt-2020-0116.
[16] Sonsino, C. M. (2007). Course of SN-curves especially in the high-cycle fatigue regime with regard to component design and safety, International Journal of Fatigue, 29, pp. 2246 – 2258, DOI: https://doi.org/10.1016/j.ijfatigue.2006.11.015.
[17] SEP1240 (2006). Testing and documentation guideline for the experimental determination of mechanical properties of steel sheets for CAE-calculations, SEP 1240:2006-07. Available at: https://www.beuth.de/en/technical-rule/sep-1240/102501063.
[18] Coffin, L. A. (1954). A study of the effects of cyclic thermal stresses on a ductile metal, Trans. ASME, vol. 76, no. 6, pp. 931–950, DOI: https://doi.org/10.1115/1.4015020.
[19] Manson, S. S. (1965). Fatigue: A complex subject – some simple approximations, Experimental Mechanics, 5(7), pp. 45-87.
[20] Basquin, O. H., (1910). The exponential law of endurance tests, Am. Soc. Test. Mater. Proc., 10, pp. 625–630, 1910.
[21] Morrow, J. D. (1965). Cyclic plastic Strain Energy and Fatigue of Metals, ASTM STP378, American Society for Testing and Materials, pp. 45–87.
[22] Wagener, R. W. (2011). Zyklisches Werkstoffverhalten bei konstanter und variabler Beanspruchungsamplitude, Ph.D. dissertation, Germany, TU Clausthal, Clausthal-Zellerfeld.
[23] Bleicher C., Pittel C., Kansy A., Niewiadomski J., Kaufmann H. (2024). Strain-life behavior of thick-walled nodular cast iron, Materialpruefung/Materials Testing, 66 (4), pp. 459 - 477, DOI: https://doi.org/10.1515/mt-2023-0307.

[24] Bleicher, C., Qaralleh, A., Fliegener, S., Sommer, S., Tlatlik, J., Kleinhans, R., Pintore, M. (2026). Influence of recycling aluminum on the quasi-static and cyclic material behavior of AlSi7Mg0.3, Procedia Structural Integrity, Volume 79, 2026, pp. 217-223, DOI: https://doi.org/10.1016/j.prostr.2025.12.327.

[25] Bleicher, C., Wagener, R., Kaufmann, H., Melz, T. (2017). Fatigue Assessment of Nodular Cast Iron with Material Imperfections, SAE International Journal of Engines, 10 (2), pp. 340 – 349. DOI: https://doi.org/10.4271/2017-01-0344.